

The Milky Way system in Λ CDM cosmological simulations

Qi Guo^{1,2}, Andrew Cooper², Carlos Frenk², John Helly², Wojciech Hellwing^{2,3}

¹ National Astronomical Observatories, Chinese Academy of Sciences, 20A Datun Road, Chaoyang, Beijing 10012, P.R. China

² Institute for Computational Cosmology, University of Durham, South Road, Durham DH1 3LE, UK

³ Institute of Astronomy, University of Zielona Góra, ul. Lubuska 2, Zielona Góra, Poland

Accepted ... Received ... in original form ...

ABSTRACT

We apply a semianalytic galaxy formation model to two high resolution cosmological N-body simulations to investigate analogues of the Milky Way system. We select these according to observed properties of the Milky Way rather than by halo mass as in most previous work. For disk-dominated central galaxies with stellar mass $(5\text{--}7) \times 10^{10} M_{\odot}$, the median host halo mass is $1.4 \times 10^{12} M_{\odot}$, with 1σ dispersion in the range $[0.86, 3.1] \times 10^{12} M_{\odot}$, consistent with dynamical measurements of the Milky Way halo mass. For any given halo mass, the probability of hosting a Milky Way system is low, with a maximum of $\sim 20\%$ in haloes of mass $\sim 10^{12} M_{\odot}$. The model reproduces the V-band luminosity function and radial profile of the bright ($M_V < -9$) Milky Way satellites. Galaxy formation in low mass haloes is found to be highly stochastic, resulting in an extremely large scatter in the relation between M_V (or stellar mass) for satellites and the depth of the subhalo potential well in which they live, as measured by the maximum of the rotation curve, V_{\max} . We conclude that the “too big to fail” problem is an artifact of selecting satellites in N-body simulations according to subhalo properties: in 10% of cases we find that three or fewer of the brightest (or most massive) satellites have $V_{\max} > 30 \text{ km s}^{-1}$. Our model predicts that around half of the dark matter subhaloes with $V_{\max} > 20 \text{ km s}^{-1}$ host satellites fainter than $M_V = -9$ and so may be missing from existing surveys.

Key words:

1 INTRODUCTION

The cold dark matter (CDM) model has been shown to be consistent with many observations on cosmological scales, but uncertainties remain on small scales where complex baryonic processes are involved. A substantial number of faint satellite galaxies are known in the Milky Way system. Thanks to their relative proximity, the distribution, chemistry and motions of their individual stars can be measured precisely. This makes the Milky Way satellites an excellent laboratory to test the CDM model and also to investigate the physics of galaxy formation on small scales.

It has been known for some time that the count of substructures in simulated Milky Way-mass dark matter haloes greatly exceeds that of the known luminous Milky Way satellites (e.g. Klypin et al. 1999; Moore et al. 1999). In the context of CDM this is readily explained if the efficiency with which baryons are converted into stars drops quickly at low halo masses. This inefficiency is expected on the basis of the well understood atomic physics governing radiative cooling, the existence of an ionising cosmic UV background, and comparison of the energy released by supernovae (which drive the expulsion of baryons from dark matter haloes) to the depth of halo potential wells (Efstathiou 1992; Kauffmann et al. 1993; Bullock et al. 2000; Benson et al. 2002; Somerville 2002).

CDM galaxy formation models which incorporate even these most basic astrophysical effects have been able to reproduce not only the abundance but also radial distribution of satellites around the Milky Way (e.g. Okamoto et al. 2010; Macciò et al. 2010; Li et al. 2010; Guo et al. 2011; Font et al. 2011; Parry et al. 2012). A host of other effects, such as cosmic ray pressure, may contribute to the regulation of star formation in these most marginal systems, (Wadepuhl & Springel 2011).

Dwarf spheroidal galaxies (dSphs) make up most of the Milky Way (MW) satellite population. Since they are dark matter-dominated galaxies, they are ideal for testing the close connection between the properties of dark matter haloes and the assembly of stellar mass predicted by CDM models. Relatively direct comparison between models and observations is now possible thanks to detailed kinematic analyses of the Milky Way dSphs (e.g. Peñarrubia et al. 2008; Strigari et al. 2008; Łokas 2009; Walker et al. 2009; Wolf et al. 2010; Strigari et al. 2010). Boylan-Kolchin et al. (2011, 2012) compared observed dSph stellar kinematics to predictions from the Aquarius Project, a set of six N-body simulations of dark matter haloes of mass $\sim 10^{12} M_{\odot}$ (consistent with constraints on the halo mass of the Milky Way; see e.g. figure 1 of Wang et al. 2014). They concluded that the most massive subhaloes in such simulations, which in typical galaxy formation models would host

the most luminous satellites, are always too dense to be dynamically consistent with observations of any of the known Milky Way companions. Boylan-Kolchin et al. (2011) dubbed this discrepancy the “too big to fail” (TBTf) problem.

Several possible solutions to the problem have been advanced, including alternative forms of dark matter (e.g. Lovell et al. 2012; Vogelsberger & Zavala 2013), baryon-induced changes in dark halo density profiles (di Cintio et al. 2011; Garrison-Kimmel et al. 2013; Arraki et al. 2013; Brooks & Zolotov 2014), and uncertainties in the mass of the Milky Way halo (Wang et al. 2012; Cautun et al. 2014). All of these studies use dark matter halo mass as a starting point to select Milky Way analogues in simulations in order to analyze the internal kinematics of their subhaloes. However, galaxy formation involves many complex processes and its outcome depends not only on the present-day halo mass, but also on the formation history of the system. This is an important consideration both for the selection of primary galaxies and for the identification of relevant satellite haloes. Indeed, Sawala et al. (2014) show that huge scatter exists in the relation between the stellar mass of dwarf satellite galaxies and their present-day subhalo mass. Sawala et al. (2014) simulated analogues of the Local Group including full baryonic physics and found that the expulsion of baryons in winds from small dark matter haloes at early times reduced the central density of the haloes in which satellites form enough to solve the TBTf fail problem.

In this paper we implement the galaxy formation model of Guo et al. (2013) on two N-body cosmological simulations and identify Milky Way analogues using the properties of their central galaxies. We compare the halo mass of these Milky Way analogues to the observations, and examine the possibility of dark matter haloes of given mass hosting the Milky Way analogues. We then further analyze the abundance and kinematics of the subhaloes of satellite galaxies selected by their luminosity or stellar mass. At the end we investigate whether selecting MW analogues according to these observables could help solve the TBTf problem.

2 SIMULATION AND SEMI-ANALYTIC MODELS

This work makes use of two Λ CDM simulations: a high-resolution zoom simulation, *Copernicus Complexio* (COCO; Hellwing et al. in prep), and a cosmological volume simulation of lower resolution, Millennium-II (MS-II Boylan-Kolchin et al. 2009). The MS-II cube has sidelength $100h^{-1}$ Mpc. The particle mass is $m_p = 6.9 \times 10^6 h^{-1} M_\odot$ and the force softening scale is $\varepsilon = 1h^{-1}$ kpc. It assumes WMAP-1 cosmological parameters, with a linear power spectrum normalization, $\sigma_8 = 0.9$, and matter density, $\Omega_m = 0.25$.

COCO simulates a high resolution comoving volume $V = 2.25 \times 10^4 h^{-3}$ Mpc³ in the centre of a lower resolution periodic cosmological cube of sidelength $70.4h^{-1}$ Mpc using $N_p = 2374^3$ DM particles. This results in a sample of ~ 50 haloes of $\sim 10^{12} M_\odot$ at $z = 0$ with high mass ($m_p = 1.135 \times 10^5 h^{-1} M_\odot$) and force ($\varepsilon = 230h^{-1}$ pc) resolution. Initial density perturbations were generated with the novel *Panphasia* technique (Jenkins 2013) which provides self-consistent and reproducible random phases for zoom-in resimulations across an arbitrary range of resolution¹.

Unlike MS-II, COCO assumes WMAP-7 cosmological parameters ($\Omega_m = 0.272$, $\Omega_\Lambda = 0.728$, $\sigma_8 = 0.81$ and $n_s = 0.968$). The slightly different cosmogonies simulated by these two calculations are reflected in the abundances and internal properties of

their dark matter haloes. For example, the abundance of MW-mass haloes differs by a few per cent (Boylan-Kolchin et al. 2011). However, the structural and kinematic properties of massive subhaloes in MW haloes are not affected in any significant way (Boylan-Kolchin et al. 2011; Wang et al. 2012; Garrison-Kimmel et al. 2013; Cautun et al. 2014).

We used stored snapshots (160 for COCO and 68 for MS-II) for Friend-of-Friends group finding (Davis et al. 1985) with a linking length equal to 0.2 times the mean inter-particle separation. Subhaloes are identified by applying the SUBFIND (Springel et al. 2001) algorithm to each FOF group. We define the centre of the FoF group as the potential minimum of the most massive self bound sub halo. The virial mass, M_{vir} , is defined as the mass enclosed by a virial radius, R_{vir} , which we approximate by the radius, R_{200} , within which the mean density is 200 times the critical value for closure. The maximum circular velocity of a halo is defined as $V_{\text{max}} = \max[\sqrt{GM(r)/r}]$ and is attained at radius r_{max} . For haloes close to the resolution limit, V_{max} can be systematically underestimated. To correct for this effect, following Springel et al. (2008), we adjust measurements V'_{max} from the simulation to $V_{\text{max}} = V'_{\text{max}}(1 + (\varepsilon/r_{\text{max}})^2)^{0.5}$.

To populate dark matter haloes in our two simulations with galaxies, we applied the semi-analytic model recently developed by the Munich Group (Guo et al. 2011, 2013) to their merger trees. This model reproduces many statistical properties of the observed galaxy population, including the abundance of bright satellites around the Milky Way (Guo et al. 2011). There are two processes crucial in understanding the formation of low mass systems: UV reionization and supernova (SN) feedback. Guo et al. (2011, 2013) adopted a fitting function originally proposed by Gnedin et al. (2004) to describe the baryon fraction as a function of halo mass and redshift. The fitting parameter and the characteristic halo mass beyond which the baryon fraction is close the universal value but below which it rapidly drops with decreasing halo mass are given by Okamoto et al. (2008).

Guo et al. (2011, 2013) introduced a SN feedback model which depends strongly on the maximum velocity of the subhalo, but the total amount of energy to reheat and eject gas can never exceed the total energy released by SNII. For most of the satellites around the Milky Way, the feedback energy saturates at this value. Guo et al. (2011) also showed that SN feedback dominates the formation of relative luminous satellites ($M_V < -11$), while reionization becomes important only for the very faint satellites ($M_V > -11$).

In Guo et al. (2011), satellite galaxies within the virial radius of their host are subject to two environmental effects: stripping of their hot gas halo by tides and ram pressure, and tidal disruption of their stellar component. The orbit of the satellite’s subhalo in the N-body simulation is used to estimate these tidal and ram pressure forces. Once a satellite galaxy loses its parent subhalo, it is considered to merge into the central galaxy unless the density of the host halo at the pericenter of the satellite’s orbit exceeds the average baryonic mass density within the half mass radius of the satellite. In this latter case, cold gas from the disrupted satellite is added to the hot gas halo of the host, and stars from the satellite to a ‘stellar halo’ component (which is not counted towards the stellar mass of the central galaxy).

In the following sections we describe how we select MW analogues from the resulting mock catalogues and present our analysis of their satellite galaxy populations.

¹ The specific COCO phase information is available on a request from the authors.

3 RESULTS

The particle mass resolution of MS-II is sufficient to study the formation history of haloes more massive than $\sim 10^{10} M_{\odot}$. Moreover, in our semi-analytic model, the properties of central galaxies in haloes of mass $10^{12} M_{\odot}$ are converged at the resolution of MS-II. However, the resolution of MS-II is not sufficient to study the internal kinematics of satellites with $V_{\max} \lesssim 30 \text{ km s}^{-1}$ (Wang et al. 2012). The resolution limit of COCO corresponds to $V_{\max} \sim 10 \text{ km s}^{-1}$ (Hellwing et al. in prep), corresponding to the least massive satellite galaxies known in the Milky Way system. The smaller volume of COCO yields relatively few Milky Way analogues, however. We therefore use the larger volume of MS-II to study the halo mass distribution of Milky Way analogues selected according to their observable properties, and the higher resolution of COCO to study the internal properties of subhaloes in systems selected in this way.

3.1 Halo mass of the Milky Way

In previous works Milky Way analogues have been identified by selecting isolated haloes with mass in a narrow range, typically around $\sim 10^{12} M_{\odot}$. However, both theoretical work (e.g. Guo et al. 2010; Moster et al. 2010; Behroozi et al. 2010; Cautun et al. 2014) and observational data (e.g. Mandelbaum et al. 2006; Leauthaud et al. 2012) suggest that the scatter in the relation between galaxy mass and host halo mass is large. This raises the question of whether or not a narrow halo mass range is sufficiently representative of the ‘Milky Way’ galaxy population.

In the following we use galaxy properties predicted by our semi-analytic model to select Milky Way analogues, rather than dark matter halo mass. Our selection is based the stellar mass and morphology of the central galaxy with the following criteria:

$$5 \times 10^{10} M_{\odot} < M_{*} < 7 \times 10^{10} M_{\odot} \quad (1)$$

and

$$0.05 < M_{\text{bulge}}/M_{*} < 0.4, \quad (2)$$

where M_{*} is the total stellar mass of the galaxy and M_{bulge} is the stellar mass of the galactic bulge. We have chosen this stellar mass range based on recent observational constraints (e.g. McMillan 2011). The bulge selection is only intended to restrict the sample to disk dominated galaxies. The actual bulge mass fraction of the Milky Way is uncertain, as is the extent to which the model ‘bulge’ mass corresponds to the photometrically or kinetically classified ‘bulges’ of real disk-dominated galaxies. This joint selection yields 566 Milky Way-like galaxies in MS-II and 13 in COCO.

In Fig. 1, the middle panel shows the distribution of M_{vir} for simulated Milky Way analogues selected according to these criteria. The black curve represents the MS-II sample and the red curve the COCO sample. Although the mass and spatial resolution of the two simulations differ greatly, a K-S test supports the hypothesis that these two samples are drawn from a common parent distribution at a confidence level of 0.97 (roughly within Poisson errors, as shown).

The median halo mass is $1.4 \times 10^{12} M_{\odot}$, with the 16th to 84th percentile range ($8.6 \times 10^{11} M_{\odot}$ to $3.1 \times 10^{12} M_{\odot}$) indicated by black dashed lines. A number of observational measurements of M_{200} are shown by symbols with error bars in the top panel of Fig. 1. These measurements have been made using the kinematics of different halo tracers by Xue et al. (2008, black circle), Gnedin

et al. (2010, blue upward triangle), Watkins et al. (2010, blue downward triangle), Sakamoto et al. (2003, cyan diamonds, with or without the inclusion of Leo I) and Battaglia et al. (2005, purple squares, assuming a truncated flat model or NFW model); using the escape velocity of the Large Magellanic Cloud or satellites (Busha et al. 2011, red diamond); using masers by Klypin et al. (2002, green circle), incorporating photometric and kinematic data by (McMillan 2011, green upward triangle); using abundance matching by Guo et al. (2010, cyan downward triangle); using the escape velocity of halo stars by Piffil et al. (2014, black rightfacing triangle); and using the timing argument of the Milky Way/Andromeda pair by Li & White (2008, red square). Almost all of the measurements in the literature fall between the 16th and 84th percentiles of the distribution predicted by our model. The model predicts that haloes of even higher masses could also host galaxies satisfying our Milky Way selection criteria: 31% of the host haloes in our samples are more massive than $2 \times 10^{12} M_{\odot}$ and 17% are more massive than $3 \times 10^{12} M_{\odot}$.

We have tested how a systematic shift in the stellar mass of the Milky Way affects the resulting halo mass distribution by assuming an alternative stellar mass range, $4 \times 10^{10} M_{\odot} < M_{*} < 6 \times 10^{10} M_{\odot}$. Relative to the peak of the black curve, we find the distribution of M_{vir} shifts to lower mass by ~ 0.1 dex. In other words, the host halo mass range does not change much if we reduce the median ‘Milky Way’ stellar mass by 20%.

The bottom panel of Fig. 1 shows the fraction of all dark matter haloes of a given mass that host a central galaxy satisfying our Milky Way selection criteria. We find that this fraction reaches a maximum of around 16% at $\sim 2 \times 10^{12} M_{\odot}$. Most of the haloes this mass either host a galaxy substantially more or less massive than the Milky Way, or else host a bulge-dominated galaxy. The fraction of Milky Ways drops rapidly at lower halo masses, and more slowly at higher masses. In general, even in the most favoured range of M_{200} , the probability for a halo of any given mass to host a MW analogue is remarkably low. Hydrodynamic simulations of disk galaxies often preselect haloes from cosmological volumes for ‘zoom’ resimulations studies based on their mass. Our results indicate that such a selection will always be inefficient. Clearly, other properties of haloes and their individual formation histories also need to be taken into account (Sawala et al. 2014).

3.2 Satellite galaxies around the Milky Way

In the last section we have shown that our model predicts a typical halo mass for Milky Way analogues in the same range as recent measurements of the Milky Way galaxy itself. In this section, we will focus on the properties and spatial distribution of satellite galaxies around the Milky Way. As mentioned in Sec. 2, the mass resolution of the COCO simulation is 60 times higher than that of MS-II, and the spatial resolution is higher by a factor of 4. More than 90% of satellites in Milky Way systems with $V_{\max} > 15 \text{ km s}^{-1}$ still have their own subhaloes in COCO, which allows us to follow their evolution in detail (see Appendix). This level of resolution is especially important for studying the internal dynamics and structure of satellite galaxies. For example, their rotation curves can be traced reliably and hence V_{\max} can be used as a robust measure of the depth of their potential. Therefore, in the following sections, we only use the COCO simulation to study the properties of satellite systems.

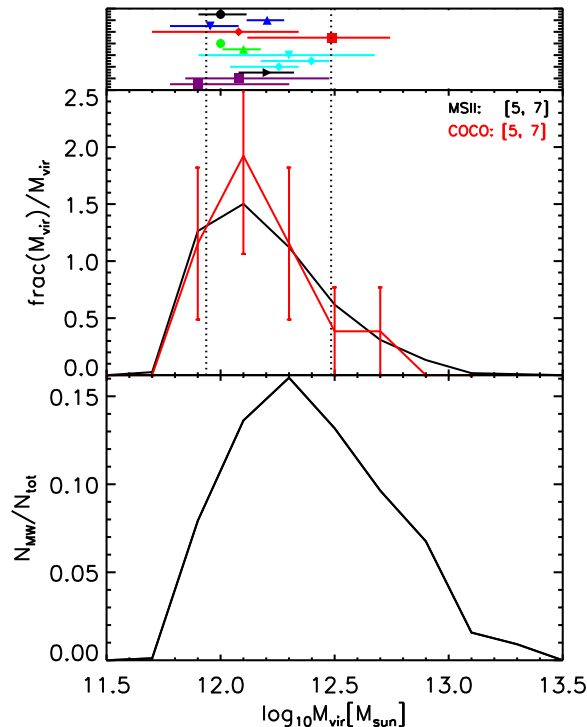


Figure 1. Upper panel: collection of measurements of M_{vir} for the Milky Way taken from the literature (see text for details). Middle panel: the distribution of host halo mass for model galaxies with $5 < M_{\star} < 7 \times 10^{10} M_{\odot}$ and $0.05 < M_{\text{bulge}}/M_{\star} < 0.4$ selected in the MS-II (black curves) and COCO (red curves) simulations. Error bars show the Poisson errors for each mass bin. A KS test supports the hypothesis of a common parent distribution in the MS-II and COCO samples at a confidence level of 0.97. Dotted lines mark the 16th to 84th percentile range of the MS-II sample. Bottom panel: the probability for a halo of a given mass to host a galaxy that matches our Milky Way criteria in MS-II.

3.2.1 Abundance and profile

Fig. 2 shows cumulative counts of satellite galaxies as a function of V-band magnitude around the 13 simulated MW analogues selected from COCO (black curves). The red dot-dashed curve represents the equivalent luminosity function of known satellites around the Milky Way and the dashed curve shows the average luminosity function of satellites in the MW and M31 found by Koposov et al. (2008), who attempted to correct for incompleteness and partial sky coverage. For this comparison, following Koposov et al., we define all galaxies within 280 kpc of each MW analogue as its satellites. The model predictions are broadly consistent with the data although the slope at the faint end is steeper in the simulations than in the data. This demonstrates convergence with the results of Guo et al. (2011), who showed that the bright end of the V-band satellite luminosity function for the much larger number of MW analogues in MS-II is also in reasonable agreement with the MW and M31 systems².

Fig. 3 compares the galactocentric radial distribution of the

² The convergence of the MS-II MW satellite luminosity functions, demonstrated here by comparison to COCO, suggests that the semi-analytic treatment of orbits for galaxies whose dark matter haloes are stripped below the resolution of the N -body simulation works reasonably well.

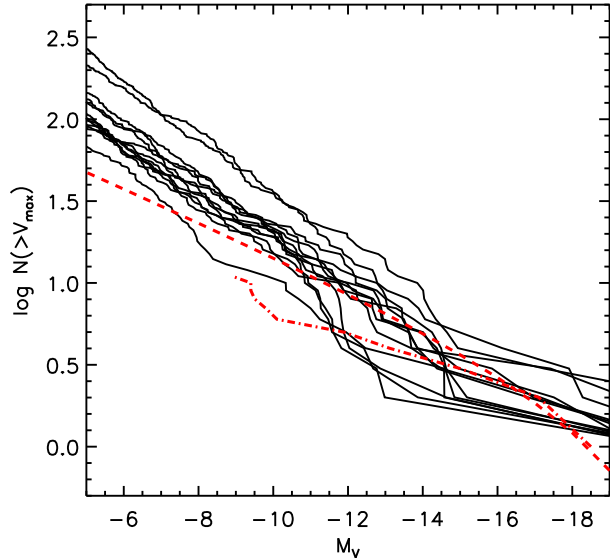


Figure 2. Cumulative distribution of V-band magnitude for satellite galaxies in each simulated MW system (black curves). The red dot-dashed line shows the equivalent distribution for known Milky Way satellites and the red dashed line the average distribution for Milky Way and M31 satellites corrected for completeness and sky coverage by Koposov et al. (2008).

most luminous satellites around our Milky Way analogues to those in the real Milky Way system. We restrict this comparison to the ‘classical’ brightest 12 satellites, using the galactocentric distances given by McConnachie (2012). These observed satellite galaxies are brighter than $M_V \approx -9$, so we select simulated satellite galaxies with $M_V < -9$ for this comparison. The Milky Way observations lie within the envelope of the radial distributions from our model.

3.2.2 Distribution of V_{max}

In the following we focus on the kinematic properties of satellite galaxies. Recently, detailed kinematic measurements have been carried out for dSphs in the Local Group (e.g. Peñarrubia et al. 2008; Strigari et al. 2008; Łokas 2009; Walker et al. 2009; Wolf et al. 2010; Strigari et al. 2010, 2014), which makes it possible to perform a relatively direct comparison between data and simulations. In particular, stellar kinematics are often used to infer V_{max} , which is then used to estimate the gravitational potentials of satellite host dark matter haloes.

V_{max} is not a direct observable, of course, and must be inferred from other properties, such as the mass within a given radius (usually the mass within the half-mass radius, $M_{1/2}$), which in turn is computed from a measured stellar velocity dispersion. To calibrate this procedure, Boylan-Kolchin et al. (2012) computed V_{max} using subhaloes from the Aquarius suite, a series of very high resolution resimulations of dark matter haloes with $M_{200} \sim 10^{12} M_{\odot}$. Assuming that the simulated subhaloes together constitute a representative sample of Milky Way-like satellite galaxy hosts, they constructed a theoretical distribution of V_{max} for each real MW satellite. This was done by assigning a weight to the V_{max} of each sim-

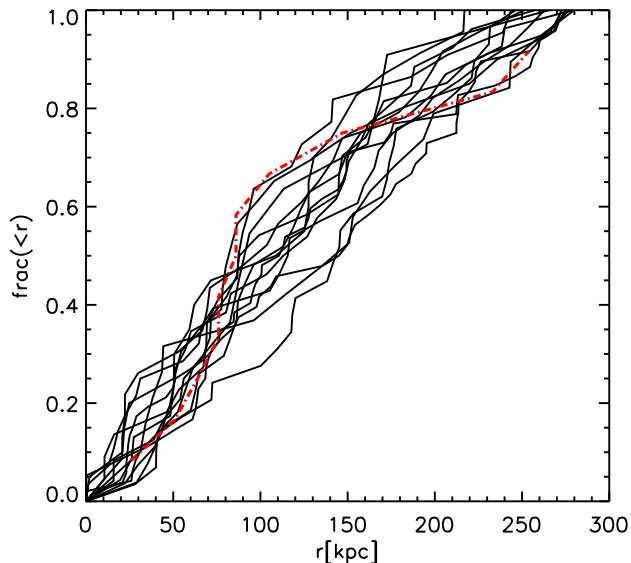


Figure 3. The radial profile of the 12 brightest Milky Way satellite galaxies (red dashed curve, McConnachie et al. 2012) compared to the profiles of satellites with $M_V < -9$ in our COCO Milky Way analogue systems (black curves).

ulated subhalo, according to how closely its mass within a radius equal to the observed stellar half-mass radius matched the value of $M_{1/2}$ inferred from kinematic observations (for details see Boylan-Kolchin et al. 2012).

Fig. 4 shows the cumulative distribution of V_{\max} for the 12 classical brightest satellites around the Milky taken from Table 2 of Boylan-Kolchin et al. (2012, red symbols with error bars)). For comparison to this data, we rank the most massive 12 satellite galaxies of each model Milky Way system according to their stellar mass and construct V_{\max} distributions (black and blue lines). The lowest value of V_{\max} corresponding to resolved satellites in COCO is about 10 km s^{-1} (see Appendix).

Most of the simulated examples overpredict the abundance of satellites with high V_{\max} relative to the Milky Way. At $V_{\max} \sim 10\text{--}15 \text{ km s}^{-1}$, predicted subhalo abundances are consistent with the MW system. At $V_{\max} \sim 17 \text{ km s}^{-1}$, several model examples still agree with the data within Poisson errors. One out of the 13 simulated Milky Way analogues has a V_{\max} distribution consistent with the data (within Poisson errors) over the whole magnitude range considered here. We mark this system with a blue curve in Fig. 4.

The host halo mass of the satellite system represented by the blue curve is $9.7 \times 10^{11} M_{\odot}$, around the median of current estimates of the MW host halo masses (Fig. 1). Hence, this is not the least massive halo in our sample. Of all our examples, this system has the lowest abundance of satellites with high V_{\max} . This may seem somewhat at odds with the conclusions of Wang et al. (2012) and Cautun et al. (2014), who found that the abundance of subhaloes at high V_{\max} is proportional to the host halo mass. Although such a relation holds on average, several factors introduce a large amount of scatter into the correlation. In particular, the luminosity of dwarf

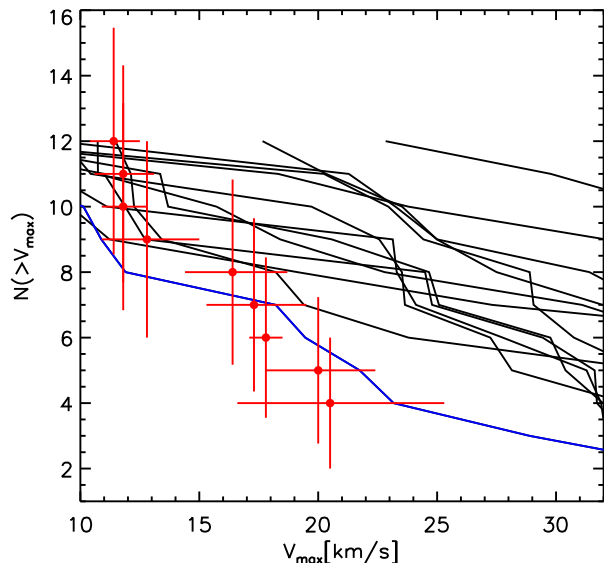


Figure 4. Cumulative distribution of maximum circular velocity for the 12 most massive satellite galaxies in each simulated MW system ranked by stellar mass (blue and black curves). Red points show the values of V_{\max} for MW satellites given by Boylan-Kochin et al. (2012). The vertical error bars on these points show the Poisson error.

galaxies in our semi-analytic model depends strongly on their formation history and not just on their present-day halo mass (e.g. Li et al. 2010). This broadens the relation between luminosity and halo mass and hence that between luminosity and V_{\max} . A similar scatter in the properties of low mass galaxies at a fixed halo mass is also found in recent hydrodynamical simulations (Sawala et al. 2014).

3.2.3 Too big to fail?

Boylan-Kolchin et al. (2011) compared the abundance of dark matter subhaloes as a function of V_{\max} in the Aquarius simulations (assumed to be a representative sample of MW host haloes) to the inferred V_{\max} distribution of Milky Way satellites. They found that Aquarius predicts significantly more subhaloes with high V_{\max} compared to what one could expect from all-sky extrapolation of the available Milky Way data. Specifically, there are only 3 known satellite galaxies with V_{\max} above 30 km s^{-1} (the Large and Small Magellanic Clouds, and the tidally disrupted galaxy in Sagittarius), whereas Aquarius predicts, on average, 8 subhaloes with $V_{\max} \gtrsim 30 \text{ km s}^{-1}$. This is one of a number of ways to express the “too big to fail” (TBTf) problem mentioned in the introduction.

Boylan-Kolchin et al. (2012) restated the TBTf problem by comparing the circular velocity profiles of simulated subhaloes to the kinematically best-matching observed MW dwarf spheroidal. Since the instantaneous value of V_{\max} for a given subhalo evolves over time (increasing as a subhalo grows, and decreasing as it is tidally stripped), they compare with values $V_{\max}(z_{\text{ref}})$ at several

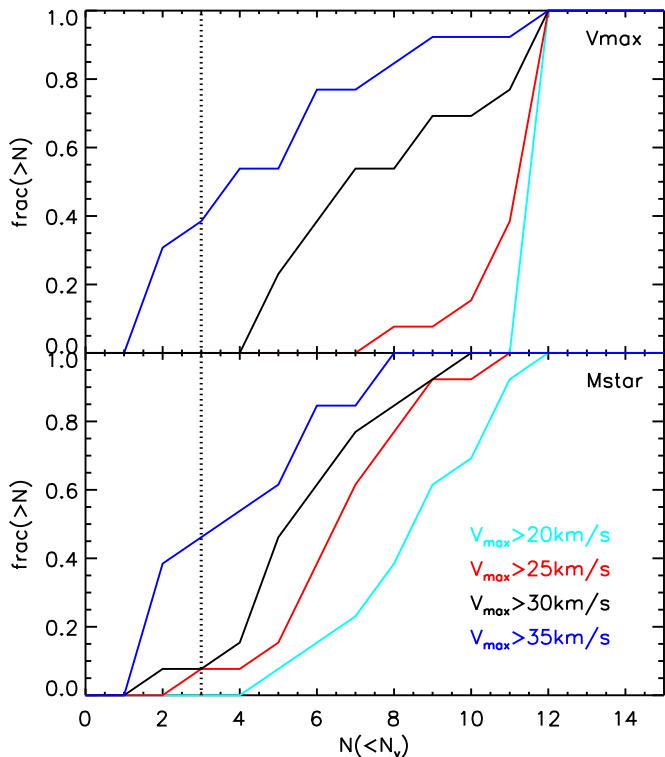


Figure 5. Cumulative distribution of maximum circular velocity for the 12 satellite galaxies with the highest V_{\max} (upper panel) and stellar mass (lower panel) in each simulated MW system, averaged over all simulated MW systems. Different colours are for different V_{\max} cuts as labelled in the right bottom corner in the bottom panel. Dotted vertical lines indicate the ‘critical number’ of three satellites.

different reference redshifts ($z_{\text{ref}} = 0, 10, z_{\text{infall}}$, etc.). The idea is that the present-day stellar mass in a subhalo should be tightly correlated with at least one choice of z_{ref} . As mentioned in the last section, however, galaxy formation in low mass haloes can be highly stochastic. Here we use the observables predicted by our model to test whether or not it suffers from a TBTF problem.

Fig. 5 shows the fraction of Milky Way analogues which host N or fewer satellites with V_{\max} greater than a threshold value (given in the legend). In the top panel, as Boylan-Kolchin et al. (2011, 2012) did, we select the 12 subhaloes with the largest values of V_{\max} at $z = 0$. We immediately see the fraction of Milky Way analogues hosting no more than $N = 3$ satellite galaxies with $V_{\max} \gtrsim 30 \text{ km s}^{-1}$ is zero, in line with the Aquarius simulations discussed above. However, assuming approximate \sqrt{N} shot noise in the real Milky Way count, we can also note that the fraction of hosts having no more than $N = 5$ subhaloes with $V_{\max} \gtrsim 30 \text{ km s}^{-1}$ is 23%.

The fraction of ‘MW-compatible’ systems decreases at a given value of N if we lower the threshold V_{\max} (red and cyan curves), and increases if we raise the threshold (blue curve). A recent study compared Local Group analogues in hydrodynamical and collisionless simulations from the same initial conditions (Sawala et al. 2014) and found that baryonic processes associated with feedback systematically reduce V_{\max} for a given subhalo by $\sim 10\% - 15\%$. As our simulation is collisionless, it is reasonable to take this effect into account by assuming observed satellites with a measured $V_{\max} = 30 \text{ km s}^{-1}$ correspond to collisionless haloes with slightly higher V_{\max} . This makes a significant difference – for example,

stating the problem in terms of subhaloes with $V_{\max} \gtrsim 35 \text{ km s}^{-1}$ yields a fraction of ‘MW-compatible’ hosts around 40%.

The TBTF problem can be further alleviated by selecting simulated satellites for comparison according to their observable properties, rather than V_{\max} . In the bottom panel of Fig. 5 we select the 12 satellites with the highest stellar mass and ask if this sample also suggests a TBTF problem. The figure shows that, even without considering the possibility that baryonic processes may reduce the values of V_{\max} , 10% of Milky Way analogues in our model have three or fewer satellites with $V_{\max} < 30 \text{ km s}^{-1}$, compatible with the real Milky Way. If systems with $N = 5$ or fewer satellites are considered comparable, then even a low V_{\max} threshold 20 km s^{-1} yields a compatible fraction of 10% (this is a very conservative threshold, since all 12 brightest satellites of the MW, except the LMC, SMC and Sagittarius, have $V_{\text{circ}} \lesssim 20 \text{ km s}^{-1}$ at their half light radius).

In summary, in addition to baryonic effects on satellite potentials and the uncertainty in the appropriate statistical error bar on the observed count of Milky Way satellites, the selection of simulated satellite galaxies by observables increases the fraction of simulated $\sim 10^{12} M_{\odot}$ haloes that have abundances of ‘high V_{\max} ’ satellites similar to that of the Milky Way system. Therefore, although lowering the assumed host halo mass alleviates the TBTF problem (Vera-Ciro et al. 2013; Wang et al. 2012; Cautun et al. 2014) this may not be necessary if a self-consistent galaxy formation model, rather than a V_{\max} scaling relation, is used to identify the ‘brightest’ satellites. This approach may be crucial for formulating realistic CDM-based theoretical predictions for MW-like satellite systems and their properties.

3.3 “Dark” substructures

The previous sections demonstrated that our model can reproduce the abundance, radial profile and V_{\max} distribution of the satellites in the Milky Way, even though the abundance of subhaloes with high V_{\max} is larger than the count of bright satellites observed with the same V_{\max} . In this section, we will show more quantitatively the diverse properties of satellite galaxies at a given V_{\max} .

3.3.1 V_{\max} vs. luminosity

The top panel of Fig. 6 shows the relation between maximum circular velocity and V-band magnitude for satellites in our 13 Milky Way analogues. The predicted median V_{\max} is an increasing function of V-band luminosity, but the scatter between V_{\max} and magnitude, M_V , is very large. Even haloes with $V_{\max} > 30$ or 20 km s^{-1} can host galaxies fainter than $M_V = -9$ (the approximate limits of completeness for current all-sky surveys of the Milky Way) or -5 , suggesting that a significant number of $20 - 30 \text{ km s}^{-1}$ satellites are still to be discovered. Likewise, at a given magnitude, V_{\max} covers a wide range. For example, at $M_V \sim -12$, V_{\max} varies from 40 km s^{-1} to $< 10 \text{ km s}^{-1}$.

This scatter between V_{\max} and luminosity stems from the fact mentioned above that the star formation rate history of a dwarf galaxy depends not only on its final halo mass or V_{\max} , but also on its dark matter mass assembly history Li et al. (2010). The bottom panel shows the relation between final stellar mass and V_{\max} measured just before the time of infall. This relation is much tighter than the stellar mass vs. present-day V_{\max} relation shown in the top panel. This is because the subhaloes hosting satellite galaxies are subject to tidal forces capable of stripping their mass. Galaxies

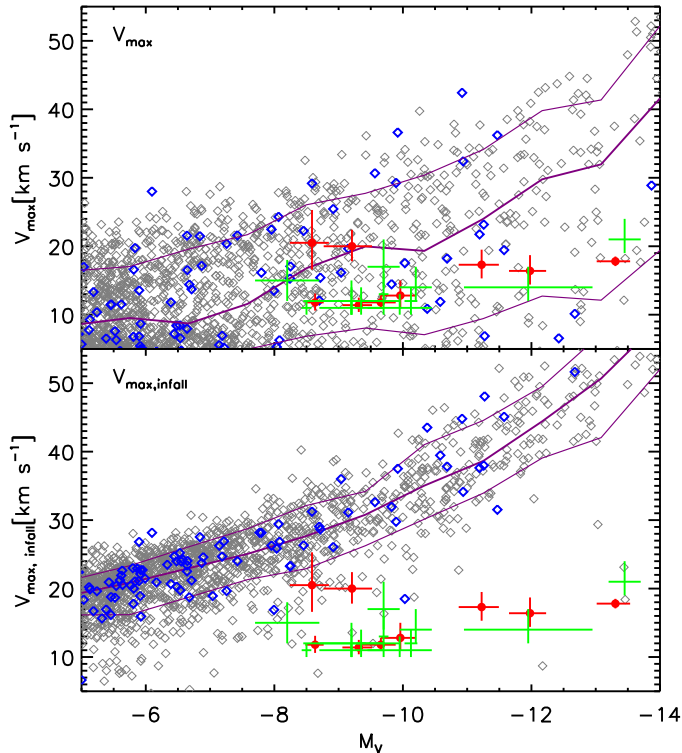


Figure 6. Top panel: V_{\max} vs. V-band luminosity for satellites of the Milky Way. Grey diamonds are our model predictions. Blue diamonds highlight satellites of the Milky Way analogue with a V_{\max} distribution consistent with the observed data over the whole magnitude range (blue curve in Fig. 4). Thick and thin purple curves give the median and 16 to 84 percent range, respectively. Bottom panel: $V_{\max,\text{infall}}$ vs. V-band luminosity for satellites of the Milky Way. The colour coding and line coding are the same as in the upper panel. Red circles with error bars are the observed MW satellites. Errors in magnitude are taken from Wolf et al. (2010), while those in V_{\max} are estimated by Boylan-Kolchin et al. (2012). Green symbols show results for satellite galaxies in M31 as given by Tollerud et al. (2014). We do not include the SMC and LMC in this figure. V_{\max} is $\sim 50 - 60 \text{ km s}^{-1}$ for the SMC (Stanimirović et al. 2004; Harris & Zaritsky 2006) and $> 80 \text{ km s}^{-1}$ for the LMC (Olsen et al. 2011). For Sagittarius, the appropriate value of V_{\max} is hard to determine, because the satellite appears to be strongly perturbed by its interaction with the central potential of the Galaxy.

embedded deep inside the potential of the substructures are more condensed and thus more resistant to such stripping, which can lower their central stellar velocity dispersion without necessarily disturbing their surface brightness profile (Peñarrubia et al. 2008; Cooper et al. 2010). Our model implies that in 1/10 of MW analogues $\sim 1 - 2$ relatively bright ($M_V \lesssim -13$) satellite galaxies may have extremely low values of V_{\max} (blue diamonds). In detail, this number will depend sensitively on the depth at which stars are embedded in their host potentials and on the details of tidal stripping.

Fig. 6 also shows the inferred relation between V_{\max} and luminosity for Milky Way and M31 satellites. V_{\max} is estimated in the same way in both cases (Tollerud et al. 2014). Most of these data lie below the median prediction of the model (thick blue curve), but well within the 16–84 percentile range. Interestingly, however, the most massive satellites in both observational datasets lie furthest below the predicted median relation.

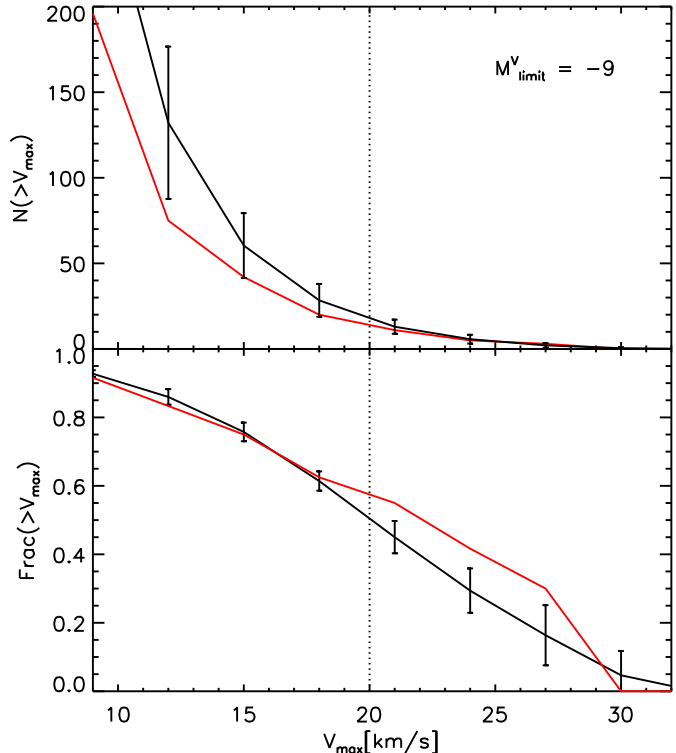


Figure 7. Upper panel: number of subhaloes with galaxies fainter than $M_V = -9$ as a function of V_{\max} . The black curve shows the median value for all 13 Milky Way analogues and the error bars show the 16 to 84 percentile range. Red curves show the one system that is consistent with the observed Milky Way satellite V_{\max} distribution, as shown in Fig. 4. Bottom panel: fraction of the subhaloes hosting galaxies fainter than $M_V = -9$ as a function of V_{\max} . The colour coding is the same as in the upper panel.

3.3.2 Detection fractions

In the last section we showed that the scatter between V_{\max} and luminosity is large, such that it is possible for relatively massive subhaloes to host a galaxy with luminosity below the current all-sky completeness limit. In this section we make an estimate of the fraction of undetected subhaloes as a function of V_{\max} . For this purpose, we consider $M_V = -9$ to be the current limit of completeness and further assume that this is a hard cut. (In practice this limit is also a function of surface brightness, and survey depth varies across the sky; e.g. Koposov et al. 2008.)

The top panel of Fig. 7 shows the average number of subhaloes hosting galaxies fainter than $M_V = -9$ as a function of V_{\max} . At 20 km s^{-1} we find a median of 18 subhaloes below this completeness limit. This corresponds to 45% of all the dark matter substructures of the same V_{\max} , as shown in the bottom panel. This fraction increases rapidly with decreasing V_{\max} , such that around 90% of subhaloes (~ 250) with $V_{\max} > 10 \text{ km s}^{-1}$ are below the limit. This conclusion holds for the single Milky Way analogue with a V_{\max} distribution consistent with Milky Way observations (red curve in Fig. 4).

4 CONCLUSIONS

We have applied a semi-analytic galaxy formation model to cosmological N-body simulations with sufficiently high resolution to study the properties of Milky Way analogues and their satellite

galaxies. Our two simulations give converged predictions for the dark halo mass of the Milky Way, despite a large difference in mass resolution (a factor of 60) and spatial resolution (a factor of 4). Given its stellar mass, the most probable value for the halo mass of the Milky Way according to our model is $1.4 \times 10^{12} M_{\odot}$, with a 1σ dispersion in the range $8.6 \times 10^{11} M_{\odot}$ to $3.1 \times 10^{12} M_{\odot}$. This median value is consistent with measurements of the Milky Way halo mass using different dynamical tracers (see Wang et al. 2015, for a summary).

For any given halo mass, the probability of hosting a Milky Way analogue is rather low, with a maximum probability of $\sim 20\%$ in haloes of mass $\sim 10^{12} M_{\odot}$. This value decreases rapidly with lower and higher host halo mass. This implies that if one wishes to simulate the formation of a Milky Way like system, halo mass selection alone is not sufficient: other factors such as environment and assembly history are important. We intend to explore the influence of such factors on the formation of Milky Way analogues in future work.

We used the COCO simulation to study the properties of satellites in Milky Way analogues. Our model is able to reproduce both the abundance of satellites as a function of V-band luminosity and the radial profile of the bright galaxies ($M_V < -9$). We have compared the V_{\max} distribution of the simulated satellites in COCO to inferences of V_{\max} from observations. We find one out of 13 V_{\max} distributions for our Milky Way analogues overlaps the observed distribution. However, we caution that the ‘observed’ values of V_{\max} are themselves dependent on calibration against collisionless N -body simulations.

With this caveat, a conservative upper limit on V_{\max} for most known satellite galaxies (excluding the LMC, SMC and Sagittarius) is $\sim 30 \text{ km s}^{-1}$. The severity of the “too big to fail” problem depends on a number of systematic uncertainties, such as the error assumed on the count of known satellites, the effect of baryonic processes on V_{\max} (Sawala et al. 2014, and references therein) and the strength of the correlation between V_{\max} and luminosity. Our model shows that this last factor – the selection of the comparison sample according to luminosity in the presence of a large scatter between luminosity and V_{\max} – is important for predicting the number of MW satellites with high V_{\max} .

The large scatter between luminosity (stellar mass) and V_{\max} is a consequence of the complex formation histories of dwarf galaxies and environmental effects (such as tidal and ram-pressure stripping) acting on dark matter subhaloes. Subhaloes with high V_{\max} can host very faint galaxies, and bright galaxies can be hosted by haloes of low V_{\max} . A significant fraction of subhaloes in our model host galaxies below the approximate all-sky completeness limit for present surveys of $M_V > -9$. Around half of our subhaloes with $V_{\max} > 20 \text{ km s}^{-1}$ host galaxies fainter than this limit. The continued discovery of fainter Milky Way companions by deeper surveys will be important for constraining even the massive end of the subhalo mass function and associated tests of the CDM model.

ACKNOWLEDGMENTS

We thank Jie Wang and Liang Gao for helpful discussion. QG acknowledges support from the NSFC grant (Nos. 11133003), the Strategic Priority Research Program The Emergence of Cosmological Structure of the Chinese Academy of Sciences (No. XDB09000000), the “Recruitment Program of Global Youth Experts” of China, the NAOC grant (Y434011V01), MPG partner

Group family, and a Royal Society Newton International Fellowship, as well as the hospitality of the Institute for Computational Cosmology at Durham University. APC is supported by a COFUND/Durham Junior Research Fellowship under EU grant [267209] and thanks Liang Gao for support in the early stages of this work under a CAS International Research Fellowship and NSFC grant [11350110323]. CSF acknowledges an ERC Advanced Investigator grant COSMIWAY [GA 267291]. This work was supported in part by the Science and Technology Facilities Council Consolidated Grant for Durham Astronomy [grant number ST/I00162X/1]. WAH is also supported by the Polish National Science Center [grant number DEC-2011/01/D/ST9/01960]. This work used the DiRAC Data Centric system at Durham University, operated by the Institute for Computational Cosmology on behalf of the STFC DiRAC HPC Facility (www.dirac.ac.uk). This equipment was funded by BIS National E-infrastructure capital grant ST/K00042X/1, STFC capital grant ST/H008519/1, and STFC DiRAC Operations grant ST/K003267/1 and Durham University. DiRAC is part of the National E-Infrastructure. The COCO simulations were run at the University of Warsaw HPC centre and we would like to thank Maciej Cytowski and Arkadiusz Niegowski for their help with these simulations.

REFERENCES

- Arraki K. S., Klypin A., More S., Trujillo-Gomez S., 2013, MNRAS
- Battaglia G., Helmi A., Morrison H., Harding P., Olszewski E. W., Mateo M., Freeman K. C., Norris J., Shtetman S. A., 2005, MNRAS, 364, 433
- Behroozi P. S., Conroy C., Wechsler R. H., 2010, ApJ, 717, 379
- Benson A. J., Frenk C. S., Lacey C. G., Baugh C. M., Cole S., 2002, MNRAS, 333, 177
- Boylan-Kolchin M., Bullock J. S., Kaplinghat M., 2011, MNRAS, 415, L40
- Boylan-Kolchin M., Bullock J. S., Kaplinghat M., 2012, MNRAS, 422, 1203
- Boylan-Kolchin M., Springel V., White S. D. M., Jenkins A., Lemson G., 2009, MNRAS, 398, 1150
- Brooks A. M., Zolotov A., 2014, ApJ, 786, 87
- Bullock J. S., Kravtsov A. V., Weinberg D. H., 2000, ApJ, 539, 517
- Busha M. T., Marshall P. J., Wechsler R. H., Klypin A., Primack J., 2011, ApJ, 743, 40
- Cautun M., Hellwing W. A., van de Weygaert R., Frenk C. S., Jones B. J. T., Sawala T., 2014, MNRAS, 445, 1820
- Cooper A. P., Cole S., Frenk C. S., White S. D. M., Helly J., Benson A. J., De Lucia G., Helmi A., Jenkins A., Navarro J. F., Springel V., Wang J., 2010, MNRAS, 406, 744
- Davis M., Efstathiou G., Frenk C. S., White S. D. M., 1985, ApJ, 292, 371
- di Cintio A., Knebe A., Libeskind N. I., Yepes G., Gottlöber S., Hoffman Y., 2011, MNRAS, 417, L74
- Efstathiou G., 1992, MNRAS, 256, 43P
- Font A. S., Benson A. J., Bower R. G., Frenk C. S., Cooper A., De Lucia G., Helly J. C., Helmi A., Li Y.-S., McCarthy I. G., Navarro J. F., Springel V., Starkeburg E., Wang J., White S. D. M., 2011, MNRAS, 417, 1260
- Garrison-Kimmel S., Rocha M., Boylan-Kolchin M., Bullock J. S., Lally J., 2013, MNRAS, 433, 3539
- Gnedin O. Y., Brown W. R., Geller M. J., Kenyon S. J., 2010, ApJ, 720, L108

- Gnedin O. Y., Kravtsov A. V., Klypin A. A., Nagai D., 2004, *ApJ*, 616, 16
- Guo Q., White S., Angulo R. E., Henriques B., Lemson G., Boylan-Kolchin M., Thomas P., Short C., 2013, *MNRAS*, 428, 1351
- Guo Q., White S., Boylan-Kolchin M., De Lucia G., Kauffmann G., Lemson G., Li C., Springel V., Weinmann S., 2011, *MNRAS*, 413, 101
- Guo Q., White S., Li C., Boylan-Kolchin M., 2010, *MNRAS*, 404, 1111
- Harris J., Zaritsky D., 2006, *AJ*, 131, 2514
- Jenkins A., 2013, *MNRAS*, 434, 2094
- Kauffmann G., White S. D. M., Guiderdoni B., 1993, *MNRAS*, 264, 201
- Klypin A., Kravtsov A. V., Valenzuela O., Prada F., 1999, *ApJ*, 522, 82
- Klypin A., Zhao H., Somerville R. S., 2002, *ApJ*, 573, 597
- Koposov S., Belokurov V., Evans N. W., Hewett P. C., Irwin M. J., Gilmore G., Zucker D. B., Rix H.-W., Fellhauer M., Bell E. F., Glushkova E. V., 2008, *ApJ*, 686, 279
- Leauthaud A., Tinker J., Bundy K., Behroozi P. S., Massey R., Rhodes J., George M. R., Kneib J.-P., et al. 2012, *ApJ*, 744, 159
- Li Y.-S., De Lucia G., Helmi A., 2010, *MNRAS*, 401, 2036
- Li Y.-S., White S. D. M., 2008, *MNRAS*, 384, 1459
- Łokas E. L., 2009, *MNRAS*, 394, L102
- Lovell M. R., Eke V., Frenk C. S., Gao L., Jenkins A., Theuns T., Wang J., White S. D. M., Boyarsky A., Ruchayskiy O., 2012, *MNRAS*, 420, 2318
- Macciò A. V., Kang X., Fontanot F., Somerville R. S., Koposov S., Monaco P., 2010, *MNRAS*, 402, 1995
- Mandelbaum R., Seljak U., Kauffmann G., Hirata C. M., Brinkmann J., 2006, *MNRAS*, 368, 715
- McConnachie A. W., 2012, *AJ*, 144, 4
- McMillan P. J., 2011, *MNRAS*, 414, 2446
- Moore B., Ghigna S., Governato F., Lake G., Quinn T., Stadel J., Tozzi P., 1999, *ApJ*, 524, L19
- Moster B. P., Somerville R. S., Maulbetsch C., van den Bosch F. C., Macciò A. V., Naab T., Oser L., 2010, *ApJ*, 710, 903
- Okamoto T., Frenk C. S., Jenkins A., Theuns T., 2010, *MNRAS*, 406, 208
- Okamoto T., Gao L., Theuns T., 2008, *MNRAS*, 390, 920
- Parry O. H., Eke V. R., Frenk C. S., Okamoto T., 2012, *MNRAS*, 419, 3304
- Peñarrubia J., Navarro J. F., McConnachie A. W., 2008, *ApJ*, 673, 226
- Piffl T., Scannapieco C., Binney J., Steinmetz M., Scholz R.-D., Williams M. E. K., de Jong R. S., Kordopatis G., et al. 2014, *A&A*, 562, A91
- Sakamoto T., Chiba M., Beers T. C., 2003, *A&A*, 397, 899
- Sawala T., Frenk C. S., Fattahi A., Navarro J. F., Bower R. G., Crain R. A., Dalla Vecchia C., Furlong M., Helly J. C., Jenkins A., Oman K. A., Schaller M., Schaye J., Theuns T., Trayford J., White S. D. M., 2014, *ArXiv e-prints*
- Sawala T., Frenk C. S., Fattahi A., Navarro J. F., Bower R. G., Crain R. A., Dalla Vecchia C., Furlong M., Jenkins A., McCarthy I. G., Qu Y., Schaller M., Schaye J., Theuns T., 2014, *ArXiv e-prints*
- Somerville R. S., 2002, *ApJ*, 572, L23
- Springel V., Wang J., Vogelsberger M., Ludlow A., Jenkins A., Helmi A., Navarro J. F., Frenk C. S., White S. D. M., 2008, *MNRAS*, 391, 1685
- Springel V., Yoshida N., White S. D. M., 2001, *New A*, 6, 79
- Stanimirović S., Staveley-Smith L., Jones P. A., 2004, *ApJ*, 604, 176
- Strigari L. E., Bullock J. S., Kaplinghat M., Simon J. D., Geha M., Willman B., Walker M. G., 2008, *Nature*, 454, 1096
- Strigari L. E., Frenk C. S., White S. D. M., 2010, *MNRAS*, 408, 2364
- Strigari L. E., Frenk C. S., White S. D. M., 2014, *ArXiv e-prints*
- Tollerud E. J., Boylan-Kolchin M., Bullock J. S., 2014, *MNRAS*, 440, 3511
- Vera-Ciro C. A., Helmi A., Starkenburg E., Breddels M. A., 2013, *MNRAS*, 428, 1696
- Vogelsberger M., Zavala J., 2013, *MNRAS*, 430, 1722
- Wadepuhl M., Springel V., 2011, *MNRAS*, 410, 1975
- Walker M. G., Mateo M., Olszewski E. W., Peñarrubia J., Wyn Evans N., Gilmore G., 2009, *ApJ*, 704, 1274
- Wang J., Frenk C. S., Navarro J. F., Gao L., Sawala T., 2012, *MNRAS*, 424, 2715
- Wang W., Han J., Cooper A., Cole S., Frenk C., Cai Y., Lowing B., 2015, *ArXiv e-prints*
- Watkins L. L., Evans N. W., An J. H., 2010, *MNRAS*, 406, 264
- Wolf J., Martinez G. D., Bullock J. S., Kaplinghat M., Geha M., Muñoz R. R., Simon J. D., Avedo F. F., 2010, *MNRAS*, 406, 1220
- Xue X. X., Rix H. W., Zhao G., Re Fiorentin P., Naab T., Steinmetz M., van den Bosch F. C., Beers T. C., Lee Y. S., Bell E. F., Rockosi C., Yanny B., Newberg H., Wilhelm R., Kang X., Smith M. C., Schneider D. P., 2008, *ApJ*, 684, 1143

APPENDIX A: NUMERICAL CONSIDERATIONS CONCERNING THE MAXIMUM CIRCULAR VELOCITY OF SATELLITES

When haloes fall into larger systems, they orbit around the potential centres as substructures, losing some of their mass to tidal stripping. Some substructures survive for a long time, while others may be disrupted shortly after infall. The finite particle mass of N-body simulations sets a minimum mass below which subhaloes cannot be resolved (in SUBFIND, subhaloes must contain at least 20 particles). Since most subhaloes lose mass through tidal stripping, many will eventually fall below this limit and be ‘lost’ from the simulation. The lower the resolution of the simulation, the more rapidly subhaloes will be lost artificially as a result of this numerical limit. The identification of the surviving substructures is thus affected by numerical resolution.

The MSII and the COCO simulations differ by a factor of 60 in particle mass and by a factor of 4 in softening length. In Fig. A1 we show the difference in the cumulative number of substructures as a function of maximum circular velocity in the two simulations. The difference is less than 20 percent at velocities, $V_{\max} > 25 \text{ km s}^{-1}$, but increases very rapidly to 100 percent at 15 km s^{-1} . At 20 km s^{-1} , MS-II resolves only half of the subhaloes found in COCO. We note that MS-II adopts a higher value of σ_8 which results in more substructures. Hence, the curve in Fig. A1 is a lower limit on the difference due to resolution. Studies of satellite kinematics with MSII should be restricted to the regime $V_{\max} > 30 \text{ km s}^{-1}$, while most of the Milky Way satellites have $V_{\max} < 20 \text{ km s}^{-1}$, except for the LMC, SMC and Sagittarius (e.g. Boylan-Kolchin et al. 2012). It is thus less reliable to use the MSII to study the properties of satellite of the Milky Way without a very

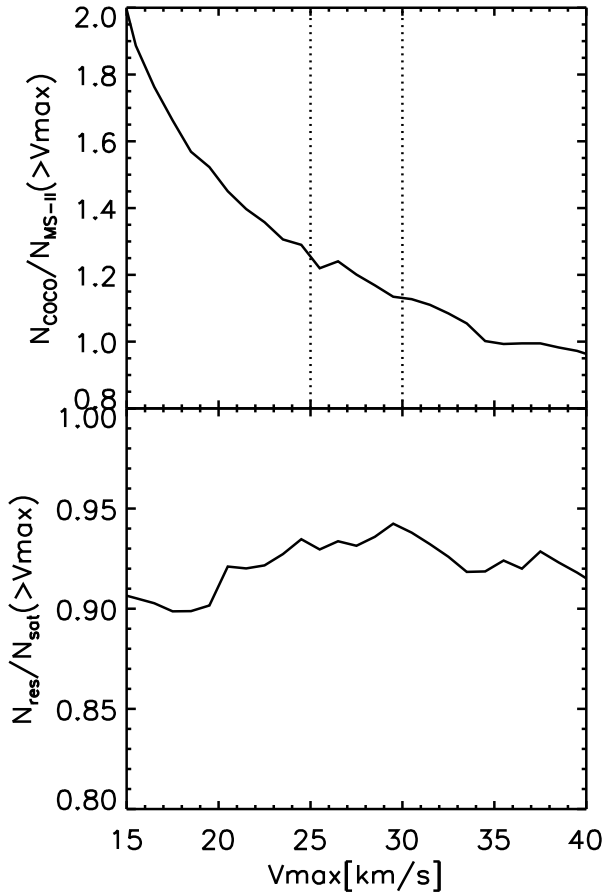


Figure A1. Upper panel: the ratio of the cumulative number of subhaloes as a function of V_{\max} in the COCO and MS-II simulations. Bottom: the ratio of the cumulative number of satellites with and without resolved subhaloes as a function of V_{\max} .

careful treatment of these satellite galaxies whose subhaloes are lost due to resolution.

The semianalytic galaxy formation model circumvents the resolution limit by allowing satellite galaxies to survive as bound objects for longer than their corresponding N-body subhaloes. We refer to these as “orphan” galaxies, because their parent subhalo has been lost. Their continued survival is determined by analytic calculations of inspiral towards the central galaxy under dynamical friction and the impact of tidal stripping on their stellar profile. The value of V_{\max} for orphan galaxies is fixed to that of their parent subhalo at the time it was last resolved. However, since these objects are suffering severe tidal stripping by definition, this estimate of V_{\max} is unlikely to be very accurate.

The bottom panel of Fig. A1 shows the fraction of satellite galaxies in our model whose subhaloes are resolved (i.e. are not orphans) as a function V_{\max} . We find more than 90 percent of satellite galaxies in COCO are in resolved subhaloes, and thus should have reliable V_{\max} measurements. In the main body of the paper we therefore use results from the COCO simulation to study satellite galaxies.